Hindawi
Shock and Vibration
Volume 2019, Article ID 7490750, 14 pages
https://doi.org/10.1155/2019/7490750

Research Article

A CBA-KELM-Based Recognition Method for Fault Diagnosis of Wind Turbines with Time-Domain Analysis and Multisensor Data Fusion

Xiafei Long,[1] Ping Yang,[2] Hongxia Guo,[1] Zhuoli Zhao,[3] and Xiwen Wu[4]

[1]*School of Electric Power, South China University of Technology, Guangzhou 510640, China*
[2]*Guangdong Key Laboratory of Clean Energy Technology, South China University of Technology, Guangzhou 510640, China*
[3]*School of Automation, Guangdong University of Technology, Guangzhou 510006, China*
[4]*Hunan New Energy Development Co.,Ltd., Guodian Power, Changsha 410016, China*

Correspondence should be addressed to Zhuoli Zhao; zhuoliscut@gmail.com

Received 3 December 2018; Revised 19 January 2019; Accepted 19 February 2019; Published 14 March 2019

Academic Editor: Enrico Zappino

Fault diagnosis technology (FDT) is an effective tool to ensure stability and reliable operation in wind turbines. In this paper, a novel fault diagnosis methodology based on a cloud bat algorithm (CBA)-kernel extreme learning machines (KELM) approach for wind turbines is proposed via combination of the multisensor data fusion technique and time-domain analysis. First, the derived method calculates the time-domain indices of raw signals, and the fused time-domain indexes dataset are obtained by the multisensor data fusion. Then, the CBA-based KELM recognition model that can identify fault patterns of a wind turbine gearbox (WTB) is automatically established with the fused dataset. The dataset includes a large number of samples involving 6 fault types under different operational conditions by 5 accelerometers. The effectiveness and feasibility of this proposed method are proved by adopting the datasets originated from the test rig, and it achieves a diagnostic accuracy of 96.25%. Finally, compared with the other peer-to-peer methods, the experimental classification results show that the proposed CBA-KELM technique has the best performances.

1. Introduction

The wind turbines [1, 2], usually working under rough and complex environmental conditions, are very vulnerable to failure throughout their lifetime [3–5]. Consequently, condition monitoring (CM) and fault diagnosis technology (FDT) for wind turbines are of vital significance not only to ensure the unit in safety running but also to reduce the operation and maintenance (O&M) costs [6]. However, the varying loads and changing environmental conditions make the CM of the wind turbines a difficult task. In order to solve these problems, many in-depth and detailed studies have been carried out recently [7–11]. It can be divided into two different kinds of classifications including qualitative diagnosis and quantitative diagnosis methods.

Among the qualitative experience approaches, in [12], it provides a method using RMS and extreme values of vibration signals for the CM of the wind turbine gearbox (WTB), but the statistical features of vibrations that characterize key condition indicators for WTB have no uniform standard. In [13], a fault diagnosis expert system of a wind turbine is established, but this method is highly dependent on expert experience. To address the aforementioned issues, in [14], a fault diagnosis technology based on the expert system and fault tree analysis is proposed, but the drawback of this approach is that it only applies to a simple wind turbine system. In [15], a signed directed graph method is adopted for fault diagnosis of wind turbines. However, it has been verified and approved only for systems with fewer loops.

Quantitative fault diagnosis, as the most common method for wind turbine fault diagnosis, includes the analytical model-based methods and the data-driven methods which are the main analytical methods. The method based on signal processing has been presented in [8, 11, 16–20]. In [8], a complex wavelet transform is proposed for multifault detection using vibration signals collected from a real wind turbine. However, the time-varying characteristics of periodic signals are not fully considered and utilized. In [11], the Hilbert transform and ensemble empirical mode decomposition method are applied to carry out fault analysis and diagnosis of a direct-drive wind turbine. However, the high computational costs and the noise pollution in the signal reconstruction by adding white noise increase the difficulty of fault diagnosis. A single senor-based blind source separation method presented in [16] has been utilized for fault diagnosis of the WTB. However, it neglects the effect of the time epoch number on the diagnostic results. In [17], bispectrum and hidden Markov model technology are applied to detect wind turbine faults, but it is shown that the complexity of this algorithm is too high.

In recent years, as the intelligent fault diagnosis algorithms, the machine learning technique has achieved enormous success. In [21, 22], the artificial neural network approach is applied to fault diagnosis. Nevertheless, the success of this method highly relies on the selection of initial threshold, weight values, and the database. Wang and Liu [23] developed a fault diagnosis strategy for wind turbine brake systems using the evidence theory, wavelet theory, and fuzzy neural network. However, how to measure the information's uncertainty affects the output of results. Bechkaoui et al. [24] and Merabet et al. [25] present the monitoring strategy of wind turbines by the fuzzy logic technique, but the accuracy of the complex model simulation system seriously affects the diagnostic effect. In [26], the extreme learning machine technique is used for fault classification of wind turbine equipment. In order to increase the accuracy of prediction, a kernel extreme learning machine (KELM) is proposed in [27–29]. KELM has a number of unique advantages, such as high learning speed, more generalized performance, and high robustness. However, it is sensitive to the parameters such as a kernel parameter and cost parameter, which may result in a low diagnostic rate.

In this paper, with time-domain analysis and multisensor data fusion technology, a variant of the basic KELM, called the cloud bat algorithm- (CBA-) based KELM, is applied for the first time to fault diagnosis of the WTB. The structure of the paper is presented as follows. Section 2 succinctly introduces the wind turbine drive train and gearbox. In Section 3, the time-domain analysis, the multisensor data fusion, and the improved KELM technology are described, and the implementation process of the proposed failure diagnosis technology for WTB is also detailed in this section. In Section 4, the validity of the proposed approach is verified using the dataset collected from the test bench. Diagnostic accuracies of the proposed approach are also compared with that of the other peer-to-peer methods. Finally, conclusions are summarized in Section 5.

2. Wind Turbine Drive Train and Gearbox

2.1. Drive Train of Wind Turbine. At present, wind power has been widely used as one of the most important promising environmentally clean energy sources. The wind turbine drive train (shown in Figure 1) is the load-bearing component in the process of energy conversion and transmission, including a rotor hub, main bearings, gearbox, and generator. The wind energy captured by the rotor hub with blades is transformed to the mechanical energy, then the main bearings transfers the mechanical energy to the generator via the gearbox that increases the lower rotor speed to a higher speed for the generator. The generator converts mechanical energy into electrical energy.

2.2. Wind Turbine Gearbox. The gearbox is a key component of the wind turbine. On the one hand, the ever-increasing capacity of wind turbines has caused the gearbox structure to become more and more complex, in the event of failure will directly lose nearly $1 million [30]. On the other hand, when it is still in the early stage of failure, due to the influence of environmental noise and other factors, the resulting fault feature components are relatively weak, resulting in the difficulty of fault diagnosis [31, 32].

Compared to any other application, the wind turbine gearboxes tend to fail early. Although their life expectancy is 20 years, it is far from meeting the requirement in the actual operation process [33]. The construction of the typical WTB which consists of two-stage bevel wheel and one-stage planetary and its transmission diagram is shown in Figure 2. The multispeed transmission is represented by three parts, namely, low, intermediate, and high speed.

Observing the pictures from Figures 3(a)–3(d), the worn tooth, tooth fracture, tooth surface deformation, and bearing faults of the WTB are demonstrated according to the results of the field investigation. Due to long-term operation of WTB under variable loads and variable speed conditions, it will lead to frequent faults and difficulty in diagnosis. In order to meet the actual situation and ensure the accuracy of the diagnosis, different kinds of faults and the same fault under different working conditions are considered in detail, including complex faults which are difficult to diagnose in this research.

3. Multisensor Data Fusion Technology and CBA-KELM-Based Fault Monitoring Technique

3.1. Time-Domain Analysis. There are a large number of vibration statistical features that characterize key condition indicators for WTB health [34, 35], such as peak index, impulse index, square root amplitude, and kurtosis. The time-domain parameters are generally divided into two types: dimensioned and dimensionless. It can judge the faults by these parameters, but different time-domain parameters behave differently for the sensitivity and stability of the fault. Moreover, there is no unified criterion for WTB vibration judgment, even if the same type of fault is judged

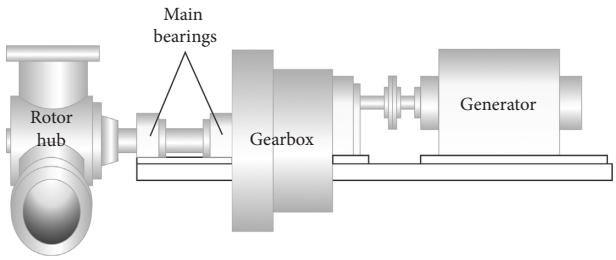

Figure 1: Drive train of a wind turbine.

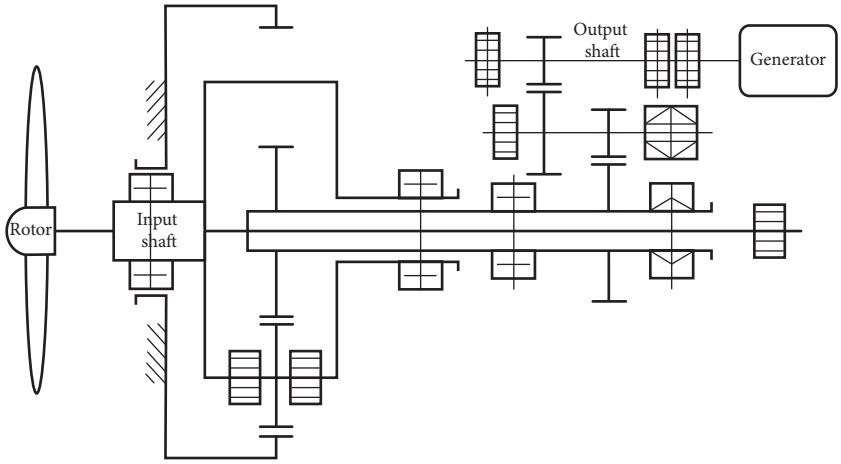

Figure 2: Structure of a wind turbine gearbox.

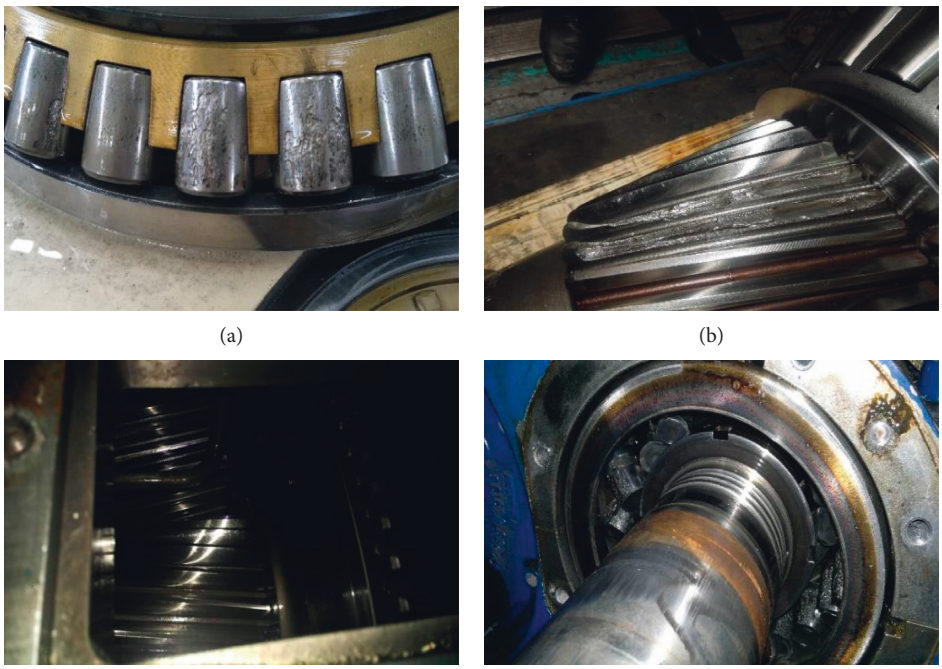

(a) (b)

(c) (d)

Figure 3: Worn tooth (a), tooth fracture (b), tooth surface deformation (c), and bearing faults (d) of the wind turbine gearbox.

on different types of wind turbines. To improve these conditions, the fault diagnosis of WTB is studied using the CBA-KELM and information fusion technology in this paper.

After collecting vibration information on the wind turbine gearbox, it can preprocess the original vibration signals by calculating the 13 different kinds of time-domain indicators (TDI), such as

$$x_{\mathrm{rms}} = \left(\frac{1}{N}\sum_{i=1}^{N}(x_i)^2\right)^{1/2}, \quad \sigma^2 = \frac{1}{N}\sum_{i=1}^{N}\left(x_i - \left(\frac{1}{N}\sum_{i=1}^{N}x_i\right)\right)^2, \tag{1}$$

$$x_{\mathrm{q}} = \frac{1}{N}\sum_{i=1}^{N}\frac{(x_i-\overline{x_i})^4}{\left((1/N)\sum_{i=1}^{N}(x_i)^2\right)^2}, \quad C = \frac{\max|x_i|}{x_{\mathrm{rms}}}, \tag{2}$$

$$I = \frac{\max|x_i|}{(1/N)\sum_{i=1}^{N}|x_i|}, \quad \overline{x_i} = \frac{1}{N}\sum_{i=1}^{N}x_i, \tag{3}$$

$$x_{\max} = \max\{x_i\}, \quad x_{\min} = \min\{x_i\}, \quad x_{\mathrm{p-p}} = x_{\max} - x_{\min}, \quad x_{\mathrm{r}} = \left(\frac{1}{N}\sum_{i=1}^{N}|x_i|^{1/2}\right)^2, \tag{4}$$

$$K = \frac{x_{\mathrm{rms}}}{x_{,}}, \quad L = \frac{\max|x_i|}{x_{\mathrm{rms}}}, \quad x_{,} = \frac{1}{N}\sum_{i=1}^{N}|x_i|, \tag{5}$$

where x_{rms} represents the root mean square value, σ^2 denotes the variance, x_{q} represents the kurtosis index, C represents the peak index, I denotes the impulse index, $\overline{x_i}$ represents the mean value, and $x_{\max}$, $x_{\min}$, $x_{\mathrm{p-p}}$, x_{r}, K, L, $x_{,}$, and N denote the maximum value, the minimum value, the peak to peak value, the square root amplitude, the waveform index, the abundance index, the average amplitude, and the length calculation of each index, respectively.

3.2. Multisensor Data Fusion Technology. With the rapid development of many different types of sensors, more and more data can be used for scientific researches. Data fusion technology is an effective way to optimize the use of multisource massive data, and it can achieve inferences that are not feasible from a source or single sensor. Three different kinds of fusion methods, namely, decision-level fusion, feature-level fusion, and data-level fusion, are introduced in detail in [36, 37].

As shown in Figure 4, in order to reduce the computational complexity and improve the fault diagnosis rate, multisensor datasets are obtained in combination with feature-level fusion and decision-level fusion technology in parallel superposition in this research. In the feature-level fusion, representative features are extracted from multisensors observation data and combined into a single connection feature vector, which is input into a pattern recognition model. The decision-level fusion involves merging information at a higher level of abstraction, combining the results of multiple sensor information to generate the final fusion decision.

As shown in Figure 5, the specific process is described as follows:

(1) Collect the vibration signals from the different acceleration sensors, and it can be defined by x_t, where n denotes the number of sensors:

$$x_t = \left\{x^1(t), x^2(t), \ldots, x^n(t)\right\}. \tag{6}$$

(2) Assuming that the finite length of discrete time series information collected from each sensor is expressed as $x^n(t) = [x_1^n, x_2^n, \ldots, x_M^n, \gamma_i^n]^T$, where γ_i^n denotes the fault classification of n_{th} sensor and M represents the data length of each sensor.

(3) According to equations (1)–(5), the original vibration signals are pretreated and analyzed, and it can get the representative feature-level information by calculating the 13 different kinds of TDI. In addition, decision-level information can also be obtained in this step.

(4) After the above steps, it obtains the dataset for each sensor, where $x^1(t)$ denotes the dataset for the first sensor. By analogy, datasets (x_t) of all sensors can be obtained through time-domain statistical analysis:

$$x^1(t) \longleftrightarrow \chi_x^1 = \begin{bmatrix} \chi_1(1,1) & \chi_1(1,2) & \cdots & \cdots & \chi_1(1,13) & \gamma_i^1 \\ \chi_1(2,1) & \chi_1(2,2) & \cdots & \cdots & \chi_1(2,13) & \gamma_i^1 \\ \vdots & \vdots & \vdots & \vdots & \vdots & \vdots \\ \chi_1(s,1) & \chi_1(s,2) & \cdots & \cdots & \chi_1(s,13) & \gamma_i^1 \end{bmatrix}.$$
$$x_t = \left\{x^1(t), x^2(t), \ldots, x^n(t)\right\} = \left\{\chi_x^1, \chi_x^2, \ldots, \chi_x^n\right\}. \tag{7}$$

(5) Combining the feature-level fusion and data-level fusion technologies, we can get the fusion dataset χ_x in parallel superposition, where $\chi_x \in R^{(M/N)\times(13\times n+1)}$, $s = M/N$. Thus, it can be defined as

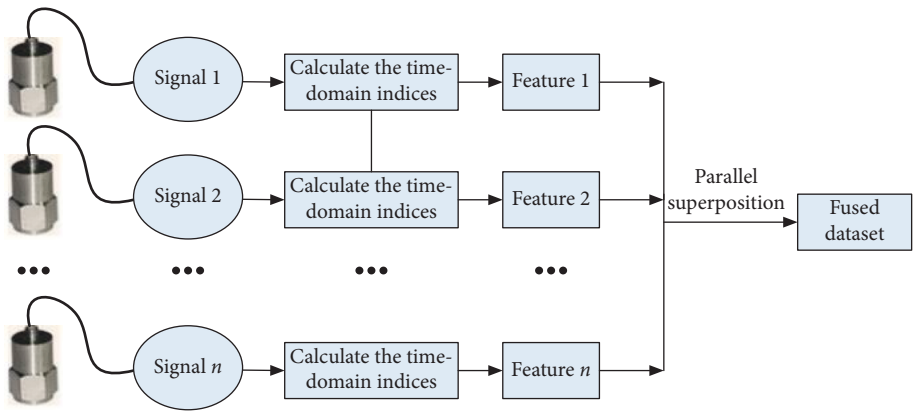

Figure 4: Framework for multisensor data fusion.

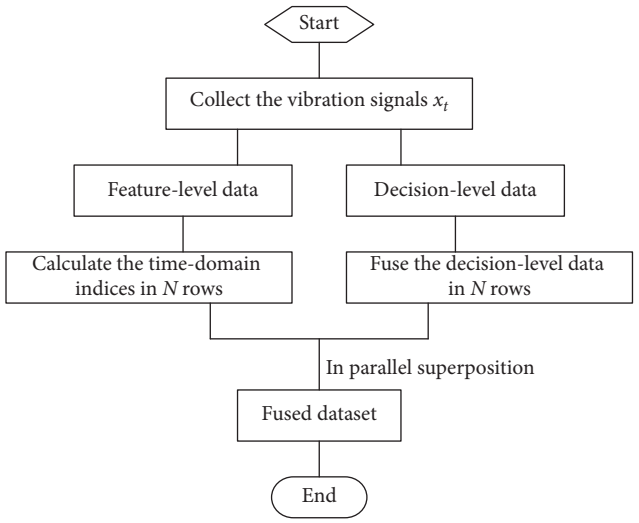

Figure 5: Flow chart of multisensor data fusion.

$$\chi_x = \begin{bmatrix} \chi_1(1,1) & \chi_1(1,2) & \cdots & \chi_1(1,13) & \cdots & \chi_n(1,13) & \gamma_i^1 \\ \chi_1(2,1) & \chi_1(2,2) & \cdots & \chi_1(2,13) & \cdots & \chi_n(2,13) & \gamma_i^1 \\ \vdots & \vdots & \vdots & \vdots & \vdots & \vdots & \vdots \\ \chi_1(s,1) & \chi_1(s,2) & \cdots & \chi_1(s,13) & \cdots & \chi_n(s,13) & \gamma_i^n \end{bmatrix}. \tag{8}$$

3.3. Kernel Extreme Learning Machine. ELM is a kind of new learning algorithm for the single-hidden layer feedforward networks (SLFNs) developed by Huang et al. [38]. Compared with the other traditional gradient-descent algorithms such as support vector machine and back propagation (BP) algorithm, the ELM tends to have better scalability and generalization performance. The architecture of an SLFN is shown in Figure 6.

Give N arbitrary distinct samples (x_i, t_i), where $t_i = [t_{i1}, t_{i2}, \ldots, t_{im}]^T$ and $x_i = [x_{i1}, x_{i2}, \ldots, x_{in}]^T$. Thus, it can be known that $\{(x_i, t_i) | x_i \in R^n, t_i \in R^m, i = 1, 2, \ldots, N\}$. In this architecture, where $w_i = [w_{i1}, w_{i2}, \ldots, w_{ik}]^T$ represents the weight vector between the i_{th} hidden node and the input nodes, $\beta_i = [\beta_{i1}, \beta_{i2}, \ldots, \beta_{im}]^T$ denotes the weight vector between the i_{th} hidden neuron and the output neurons, y_j represents the outputs of the network, b_i is the threshold of neurons in the i_{th} hidden layer, n, k, and m indicates the number of nodes in the input layer (hidden layer/output layer), respectively, and $g(x)$ denotes the sigmoid function.

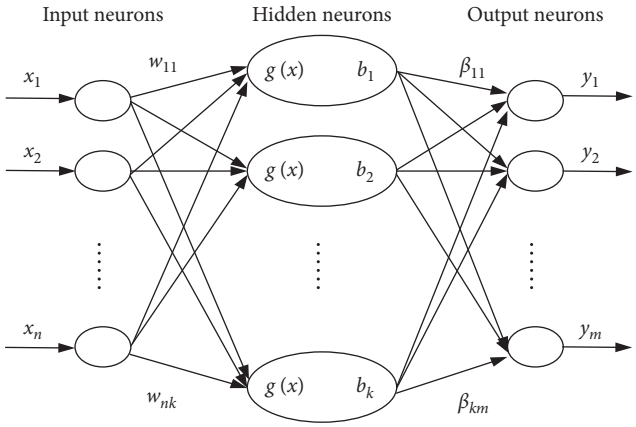

Figure 6: Architecture of an SLFN.

The ELM classifier can be expressed as the following equation:

$$\begin{aligned} y_j &= \sum_{i=1}^{k} \beta_i g_i(x_j) = \sum_{i=1}^{k} \beta_i g(w_i \cdot x_j + b_i) \\ &= \sum_{i=1}^{k} \beta_i h_i(x) = h(x)\beta_j, \quad j = 1, 2, \ldots, m. \end{aligned} \tag{9}$$

With zero error means, the SLFNs with k hidden neurons can approximate these N samples that $\sum_{j=1}^{k} \| y_j - t_j \| = 0$. Thus, it can know that there exist b_i, w_i, and β_i, which can be described as

$$\sum_{i=1}^{k} \beta_i g(w_i \cdot x_j + b_i) = t_j, \quad j = 1, 2, \ldots, N. \tag{10}$$

Then, its compact version can be fully expressed as

$$H\beta = T, \tag{11}$$

where

$$H(w_1, w_2, \ldots, w_k, b_1, b_2, \ldots, b_k, x_1, x_2, \ldots, x_N) = \begin{bmatrix} g(w_1 \cdot x_1 + b_1) & \cdots & g(w_k \cdot x_1 + b_k) \\ \vdots & \cdots & \vdots \\ g(w_1 \cdot x_N + b_1) & \cdots & g(w_k \cdot x_N + b_k) \end{bmatrix}_{N \times k},$$
$$\beta = \begin{bmatrix} \beta_1^T \\ \vdots \\ \beta_k^T \end{bmatrix}_{k \times m}, \tag{12}$$
$$T = \begin{bmatrix} t_1^T \\ \vdots \\ t_N^T \end{bmatrix}_{N \times m}.$$

Thus, the output layer weight vector can be denoted by equation (13) according to the basic theory of ELM, where H^* represents the Moore–Penrose generalized inverse matrix, which can be described in equation (14) and C is called the cost parameter, related to the stability and generalized performance:

$$\beta = H^* T, \tag{13}$$

$$H^* = H^T \left(\frac{I}{C} + HH^T \right)^{-1}. \tag{14}$$

Because the feature mapping H do not need to know to users, a kernel-based ELM is applied for improving learning speed, generalized performance, and accuracy of judgment in this paper. The KELM algorithm is an improved algorithm in combination with the kernel function on the proposed ELM algorithm. Thus, the kernel matrix and the output function of the ELM classifier can be denoted by equations (15) and (16), respectively. And the radial basis function kernel is chosen as follows (equation (17)), where γ is the kernel parameter:

$$\Omega_{\text{ELM}} = HH^T \ : \ \Omega_{\text{ELM}_{ij}} = h(x_i) h(x_j) = K(x_i, x_j), \tag{15}$$

$$y = h(x) H^T \left(\frac{I}{C} + HH^T \right)^{-1} T = \begin{bmatrix} K(x, x_1) \\ \vdots \\ K(x, x_N) \end{bmatrix} \cdot \left(\frac{I}{C} + \Omega_{\text{ELM}} \right)^{-1} T, \tag{16}$$

$$K(x, y) = \exp\left(- \frac{\|x - y\|^2}{2\gamma^2} \right). \tag{17}$$

3.4. Kernel Extreme Learning Machine Optimized Cloud Bat Algorithm. Due to the existence of the kernel function, this algorithm is sensitive to parameter setting. The parameters γ and C have a significant influence on the performance of the algorithm when executing the KELM learning algorithm. The CBA algorithm [39] not only has the advantages of the bat algorithm (BA) but also has other advantages such as reduction of the loudness, increasing of the pulse rate emission, and strong stability. Therefore, γ and C are optimized using the CBA algorithm to create a CBA-optimized KELM prediction model. The CBA algorithm which takes the bat echolocation predation mechanism as the starting point and takes the universality of the normal cloud model as the basis is proposed in this research. Suppose the KELM classification accuracy as $\text{pre}(C, \gamma)$. Thus, within a given range, it needs to be guaranteed to get the maximum classification accuracy as follows:

$$R = \max \text{pre}(C, \gamma). \tag{18}$$

The proposed algorithm of the CBA-KELM can be described as follows:

(1) Randomly initialize the relevant parameters, evaluate the initial positions using the fitness function, and search for a population elite x_{pbest}.

(2) Generate the drops of the cloud based on the information provided by the current optimal solution. $\text{pbc}_i(E_x, E_n, H_e)$ represents the population bats cloud, here $H_e = E_n/c2$, $E_x = x_{\text{pbest}}$, and $E_n = (\text{AVG}(\sum \text{rate}_i) - x_{\text{pbest}})/c1$, AVG represents the averaging function, $c1$ and $c2$ are the learning factor.

(3) The individual experience x_{ebest} for each bat and x_{pbest} is obtained in each step. Thus, the optimal position for each group is $g(i)_{\text{best}} = [C_i^{\text{best}}(t), \gamma_i^{\text{best}}(t)]^T$.

(4) The pulse rate, velocity, and position are updated adopting the following equations:

$$f_i = f_{\min} + (f_{\max} - f_{\min})\beta,$$
$$V_i^t = V_i^{t-1} + \left(X_i^T - x_{\text{pbest},i}\right) f_i, \quad (19)$$
$$X_i^t = X_i^{t-1} + V_i^t,$$

where β is a random digit in the range [0, 1], the pulse frequency range is defined by $[f_{\min}, f_{\max}]$, X_i^t denotes the position of the bat, and V_i^t represents the velocity of the bat.

(5) Steps (2)–(4) are executed until the predefined maximum number of optimizing generation is satisfied.

Compared with the KELM method, the CBA-KELM is verified more effectively by using the same sample in this section. The programs are run in the MATLAB R2017a environment, and the results are shown in Figure 7. Obviously, the CBA-KELM has a better performance.

3.5. CBA-KELM-Based Fault Monitoring Technique for Wind Turbines. According to the previous discussion, the $13n$ parameters are chosen to form the feature vector, including the signals collected from n different sensors. In this paper, the raw signals originated from five sensors in different locations containing six types of faults. The KELM-based SLFN fault diagnosis model is established and illustrated in Figure 8, which has 65 inputs and six outputs. Based on the labeled fused dataset, the SLFN neural network is trained according to the learning algorithm supported by the CBA-KELM algorithm. As shown in Figure 9, the application of the CBA-KELM method for the WTB fault diagnosis can be summarized as follows:

Step 1. Collect the vibration signals x_t from the sensors mounted on the WTB, and the fault classification is defined according to different faults.

Step 2. In order to obtain the fused dataset, the TDI index of $x^n(t)$ is calculated. Thus, we can get the χ_x matrix from the original vibration signal using equations (1)–(6), and the feature level fusion and data level fusion technology are merged in a way of parallel superposition.

Step 3. Normalize the fused datasets. It can obtain the preprocessed data samples to test or train the fault diagnosis model after normalizing the fused datasets.

Step 4. Divide the data samples. The ratio of the testing dataset and training dataset is randomly set. The testing samples are applied to validate the fault diagnosis model, and the training samples are adopted to train this model.

Step 5. Optimize the KELM parameters. The KELM parameters γ and C play an important role in accuracy and generalization, so they are optimized by using the CBA algorithm in this step.

Step 6. Obtain the fault diagnosis model using the CBA-KELM approach. It can judge the fault type when employing the fault diagnosis model.

4. Experimental Verification

In order to correctly verify the proposed method, the raw vibration signals of the faulty gearbox originated from Qian Peng Company's rotating machinery vibration analysis and fault diagnosis test platform system [40]. The wind power gearbox runs in a harsh environment for a long time and works under different loads and rotational speeds. Therefore, the experimental device takes these conditions into full consideration and simulates the gearbox faults under different loads and rotating speeds. The collected data reflect the various fault types of the gearbox, including not only single faults such as pitting tooth, worn tooth, and tooth fracture but also comprehensive composite faults that are difficult to diagnose, which is consistent with the actual operation of the gearbox in a wind farm. The presented CBA-KELM method is then used in the fault diagnosis, and different kinds of methods are also shown for the comparative analysis.

4.1. Data Acquisition and Preprocessing. The test platform system, which has the 5.12 kHz sampling rate, consists of a variable-speed drive motor, bearings, gearbox, shafts, and so on. Various faults can be quickly simulated by adjusting the counterweight, the installation position of the parts, and the organic combination of components. The map diagram of this test platform system is shown in Figure 10. It can complete the collection of on-site vibration signals and has the following functions: signal acquisition, real-time display, signal preservation, etc. The gearbox used for the experiment is a decelerator. An input gear ($N_{Z_1} = 55$, modulus = 2) is installed on the input shaft, and an output gear ($N_{Z_2} = 75$, modulus = 2) is mounted on the output shaft, where Z_1 and Z_2 represent the pinion gear and the large gear, respectively. And N_{Z_1} and N_{Z_2} are the number of teeth of the pinion and the large gear.

In this research, six gearbox failures (i.e., $\gamma_i^n = \{1, 2, 3, 4, 5, 6\}$) were simulated at different rotational speeds and loads, including complex faults which are difficult to diagnose. The detailed explanation of the dataset is shown in Table 1. The original vibration signals originate from five accelerometers (sensor 1–5) mounted at different positions on the gearbox, namely, input shaft motor-side bearing, the output shaft motor-side bearing, the input shaft load-side bearing, the output shaft load-side bearing Y, and the output shaft load-side bearing X. In addition to the five accelerometers, a sensor (sensor 6) for measuring the gearbox input shaft speed is installed. The magnetic powder torque device shown on the test bench can automatically adjust the torque. Corresponding to six kinds of fault classification, 6,064,640 vibratory signals are collected. Thus, the total datasets are obtained from the gearbox fault diagnosis experiments.

Using the proposed approach, the raw signals are preprocessed. According to the time-domain analysis, the initial matrix set is converted to another matrix. The time-domain parameters are calculated in rows of 512. In parallel superposition way, the feature level and data level are merged

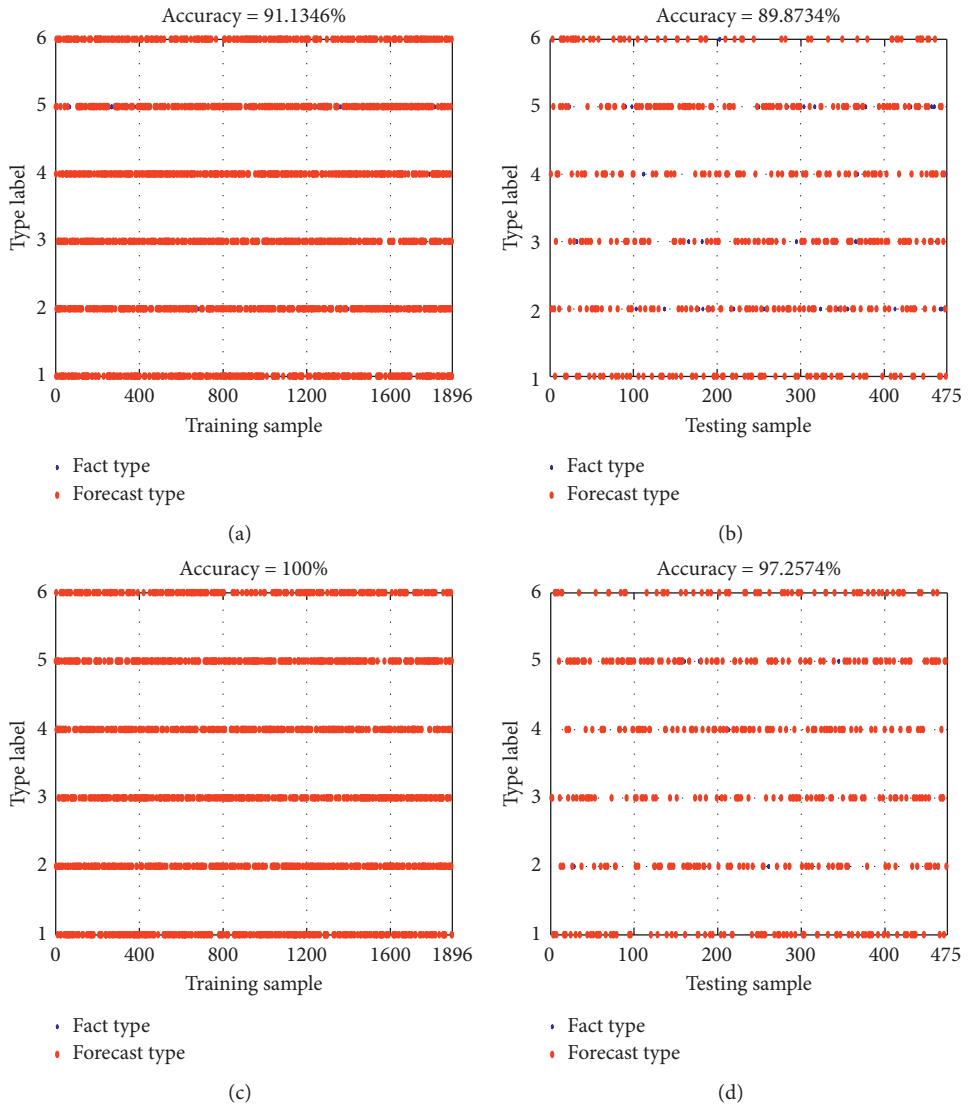

Figure 7: The diagnostic accuracy of the KELM technique with (a) the training sample and (b) the test sample. The diagnostic accuracy of the CBA-KELM method with (c) the training sample and (d) the test sample.

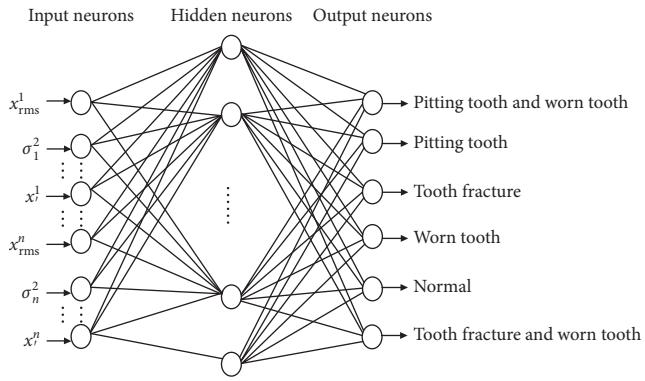

Figure 8: The CBA-KELM-based SLFN fault diagnosis model.

at the same time. Hence, a fused domain matrix with 2369 lines and 66 columns is obtained. The fused time-domain matrix is used to train the KELM model.

4.2. Experimental Results. The CBA-KELM-based method is used to identify the fault classification of gearboxes with the multisensor fusion. The CBA-KELM model is developed with the following parameters: 13 different kinds of time-domain indicators are calculated for fused datasets; the number of the neurons in the input layer is 65; the number of the neurons in the output layer is six; the kernel function is the radial basis function (RBF); the number of iterations is determined to be 100; the acceleration coefficient is identified as $c1 = c2 = 1.49445$; the population number is set as 10; and the parameter ranges of γ and C are [0.1, 10] and [0, 1000], respectively.

To train the CBA-KELM model, trials are repeated 20 times, where 80% of the data samples are randomly exploited to be as the training dataset, and the remaining 20% data samples are used as the testing dataset. When applying the CBA method for KELM approach, the KELM parameters γ and C should be determined after optimization. The fault

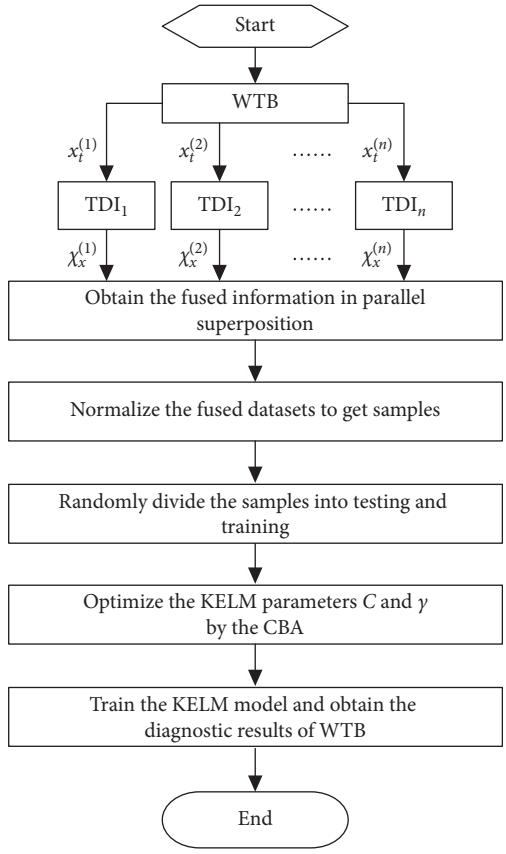

Figure 9: Schematic structure of the proposed CBA-KELM model.

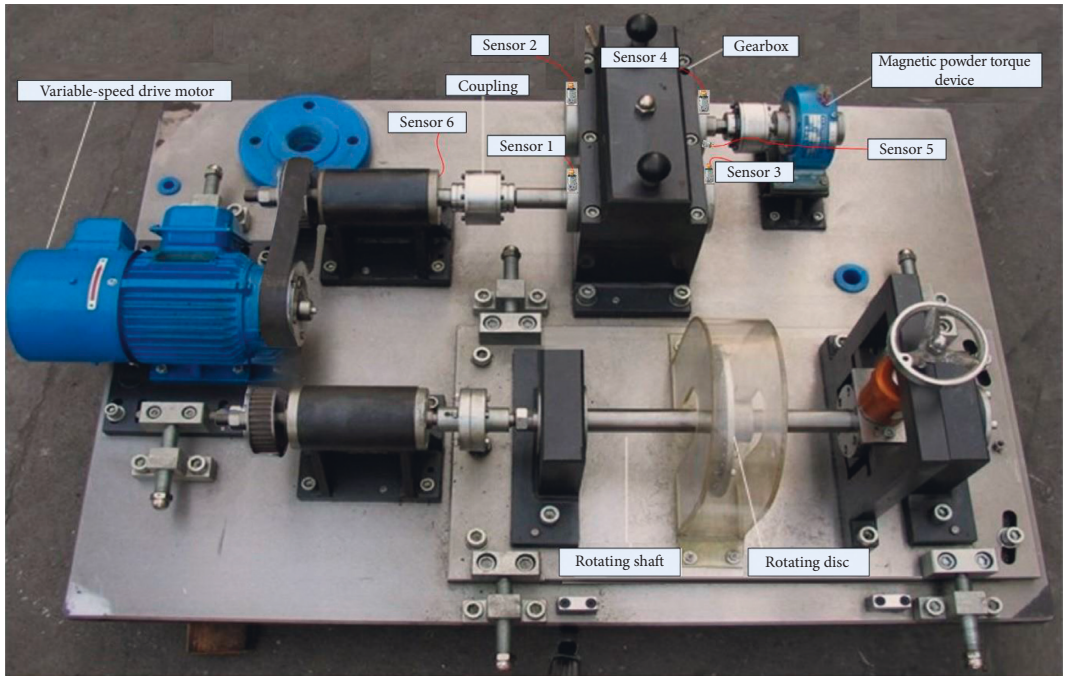

Figure 10: The test platform system.

classification results of these 20 times using the proposed CBA-KELM based method are shown in Figure 11(a). Among all these trails, the average training accuracy is 100%, and the average testing accuracy is 96.25%, which means that the fault diagnosis and classification have higher accuracy based on the method shown in Table 2.

Table 1: Description of the dataset.

Faulty component	Rotating speed (rpm)	Fault type	Load (hp)	Label of classification
Gear Z_1 Gear Z_2	1470, 880, 825, 849	Pitting tooth Worn tooth	0, 0, 0.14, 0.07	1
Gear Z_1	1500, 880, 834, 850	Pitting tooth	0, 0, 0.14, 0.07	2
Gear Z_1	1470, 878, 840, 860	Tooth fracture	0, 0, 0.14, 0.07	3
Gear Z_2	1478, 881, 830, 854	Worn tooth	0, 0, 0.14, 0.07	4
Normal	1475, 880, 800, 820	Normal	0, 0, 0.14, 0.07	5
Gear Z_1 Gear Z_2	1474, 878, 812, 842	Tooth fracture Worn tooth	0, 0, 0.14, 0.07	6

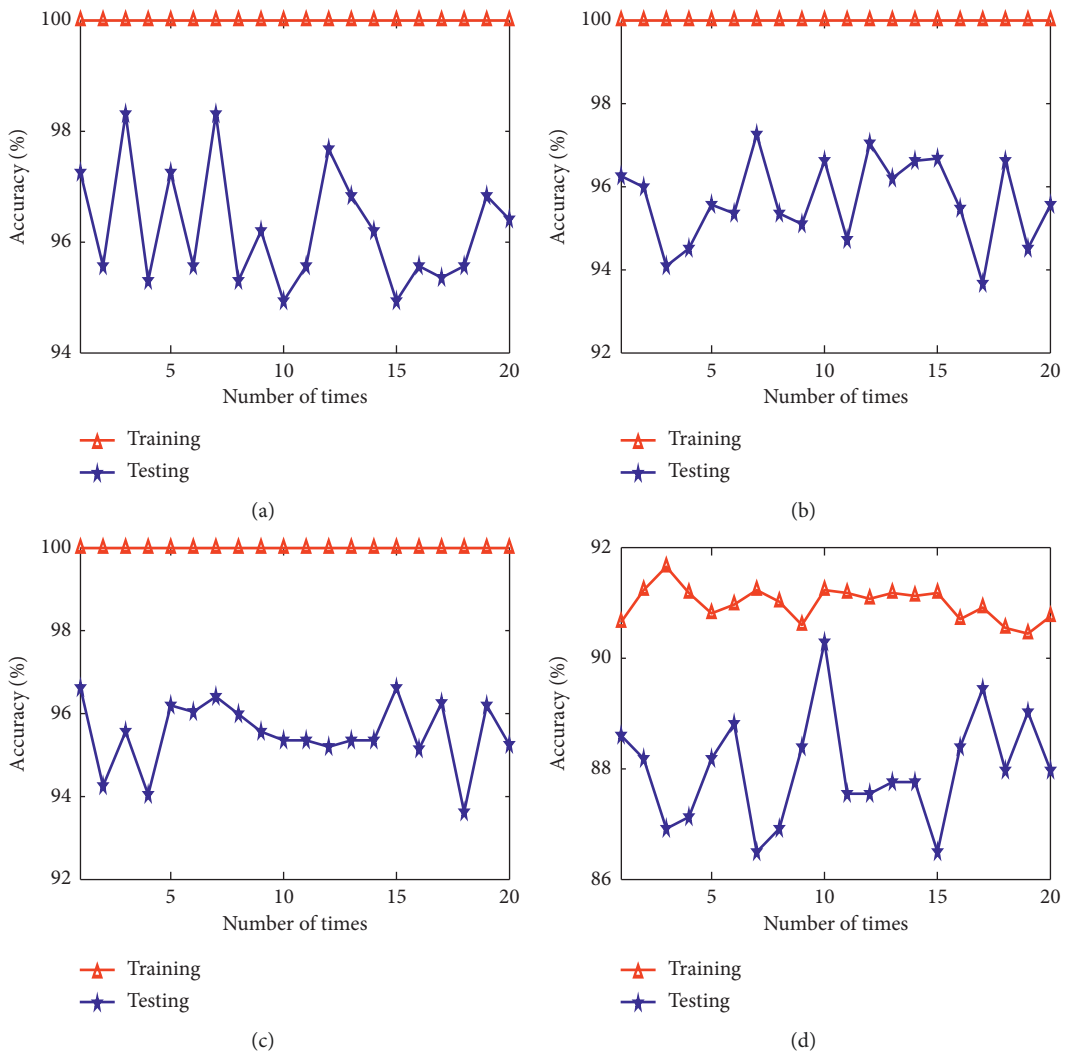

Figure 11: Continued.

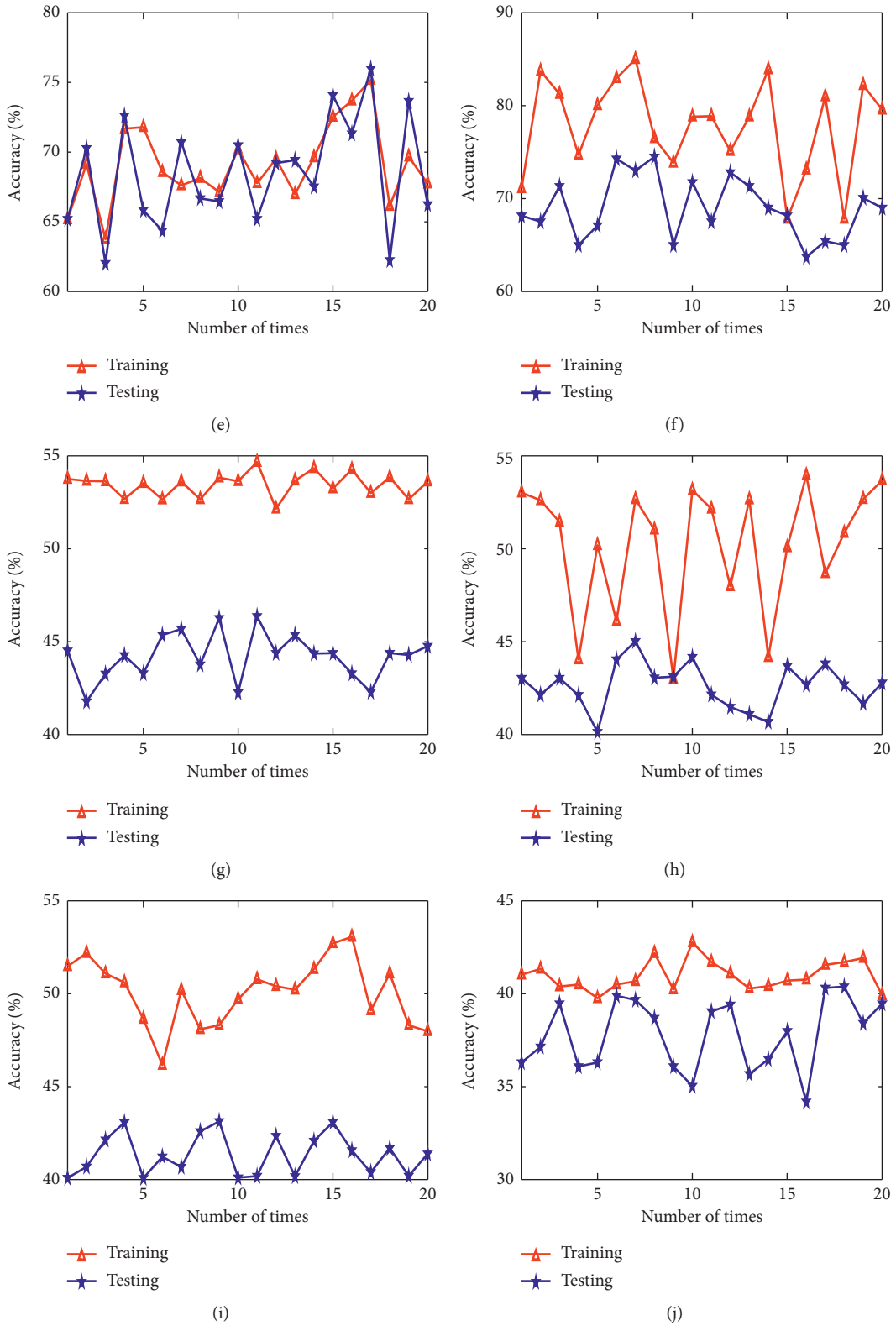

Figure 11: Continued.

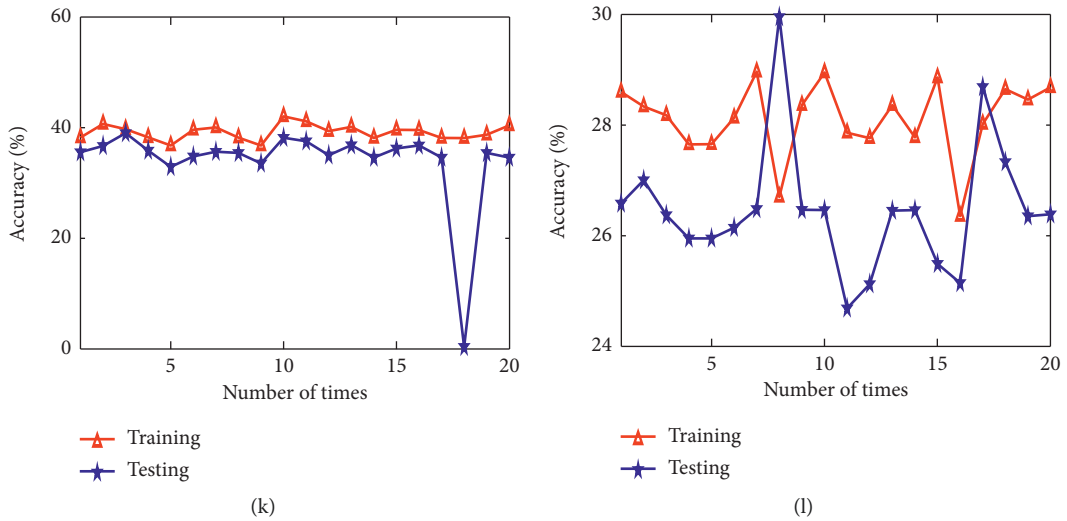

Figure 11: Fault diagnosis results: (a) CBA-KELM, (b) BA-KELM, (c) FA-KELM, (d) KELM, (e) ELM, and (f) BPNN methods with the fused dataset; (g) CBA-KELM, (h) BA-KELM, (i) FA-KELM, (j) KELM, (k) ELM, and (l) BPNN methods with the unfused dataset.

Table 2: Comparisons with peer-to-peer classification.

Methods	Data type	Average training accuracy (%)	Average testing accuracy (%)
The proposed CBA-KELM method	Fusion data	100	96.25
	Raw data	53.47	44.22
The proposed BA-KELM method	Fusion data	100	95.66
	Raw data	50.22	42.63
The proposed FA-KELM method	Fusion data	100	95.52
	Raw data	50.05	41.34
The KELM method	Fusion data	90.99	87.90
	Raw data	40.95	37.79
The ELM method	Fusion data	69.06	68.46
	Raw data	39.20	33.99
The BPNN method	Fusion data	77.78	68.97
	Raw data	28.12	26.47

4.3. Comparisons and Discussion. The proposed BA-KELM method utilizing the fused dataset is introduced in this paper. All the parameter settings are selected the same as the CBA algorithm except that the cloud theory is not used to optimize the weight of the BA algorithm. To train the BA-KELM model, the experiment is also repeated 20 times, with 80% of the data samples being used randomly as the training datasets and the remaining being used as the test datasets. Using the BA-KELM algorithm, the fault classification results of these 20 experiments are shown in Figure 11(b). Among these experiments, the average training accuracy rate is 100%. And the average testing accuracy rate is 95.66%, which is lower than the CBA-KELM approach.

The FA technique is a new type of bionic intelligent algorithm, which originates from the group behavior of fireflies in the natural world through information exchange. The FA-KELM model has the same parameter settings as the CBA-KELM method and the BA-KELM technique. From Figure 11(c), it can be known that the average training accuracy is 100% and the average testing accuracy is 95.52%.

The KELM algorithm, which is implemented in a single learning step, and the parameters are usually assigned based on experience or trajectory [41]. Its parameter settings are the same as those in the KELM model in BA-KELM and CBA-KELM algorithms. After 20 trials, the average training accuracy reaches 90.99% and the average testing accuracy reaches 87.90%, as shown in Figure 11(d).

The ELM model is developed with the following parameters: 13 different kinds of time-domain indicators are calculated for fused datasets; the number of the neurons in the input layer is 65; the number of the neurons in the output layer is six; and the number of the neurons in the hidden layer is 10. In order to train the ELM model, the experiment is repeated 20 times, 80% of the data samples are randomly used as training datasets and the rest are used as test datasets. After 20 trials, the fault classification results are shown in Figure 11(e). The average training accuracy and average testing accuracy are 69.06% and 68.46%, respectively.

The parameters of the BPNN-based technique are set as follows: the number of the input layer and output layer are set as one; the number of hidden layers is set as two; the number of input and output neurons is determined as 65 and 6, respectively; the number of the first and the second hidden layers is set as 14. Trails also are repeated 20 times, and the

fault classification results using this method are shown in Figure 11(f). It is shown that the average training accuracies are 77.78% and the average testing accuracies are 68.97%.

In Figures 11(g)–11(l), the CBA-KELM, BA-KELM, FA-KELM, KELM, ELM, and BPNN algorithms based on unfused datasets are applied in this paper. The average training accuracies and training accuracies are very poor, no more than 55%. This denotes that the fused signals of these multisensors are more meaningful, which can fully reflect the fault condition. The classification results prove that information fusion technology can improve fault diagnosis accuracies.

5. Conclusions

This paper presents a novel approach for FDT of a wind turbine gearbox based on CBA-KELM with time-domain analysis and multisensor data fusion technology. In combination with feature-evel fusion and data-level fusion technology in parallel superposition, the original vibration signal is preprocessed in order to obtain the fused datasets. The fused datasets contain a large number of samples involving six classifications by five accelerometers, including complex faults which are difficult to diagnose. And a fault classification method of KELM is optimized by using the CBA algorithm, which can obtain a high accuracy. The validity of the proposed FDT method is proved by using the fused data collected from the test platform system from the Qian Peng Company. Compared with a variety of other peer-to-peer methods, the proposed approach has the highest accuracy and stability.

Data Availability

The data used to support the findings of this study are available from the corresponding author upon request.

Conflicts of Interest

The authors declare that there are no conflicts of interest regarding the publication of this paper.

Acknowledgments

This research was supported in part by the National Science and Technology Support Program (Grant No. 2015BAA06B02), by the Science and Technology Planning Project of Guangdong Province (Grant No. 2016B020245001), and by the Operation Fund of Guangdong Key Laboratory of Clean Energy Technology (Grant No. 2017B030314127).

References

[1] R. Jia, F. Ma, J. Dang, G. Liu, and H. Zhang, "Research on multidomain fault diagnosis of large wind turbines under complex environment," *Complexity*, vol. 2018, Article ID 2896850, 13 pages, 2018.

[2] X. Long, P. Yang, H. Guo, and X. Wu, "Review of fault diagnosis methods for large wind turbines," *Power System Technology*, vol. 41, no. 11, pp. 3480–3491, 2017.

[3] M. L. Wymore, J. E. Van Dam, H. Ceylan, and D. Qiao, "A survey of health monitoring systems for wind turbines," *Renewable and Sustainable Energy Reviews*, vol. 52, pp. 976–990, 2015.

[4] R. Bajric, N. Zuber, G. A. Skrimpas, and N. Mijatovic, "Feature extraction using discrete wavelet transform for gear fault diagnosis of wind turbine gearbox," *Shock and Vibration*, vol. 2016, Article ID 6748469, 10 pages, 2016.

[5] X. Chen and Z. Feng, "Application of reassigned wavelet scalogram in wind turbine planetary gearbox fault diagnosis under nonstationary conditions," *Shock and Vibration*, vol. 2016, Article ID 6723267, 12 pages, 2016.

[6] A. Romero, Y. Lage, S. Soua, B. Wang, and T.-H. Gan, "Vestas V90-3MW wind turbine gearbox health assessment using a vibration-based condition monitoring system," *Shock and Vibration*, vol. 2016, Article ID 6423587, 18 pages, 2016.

[7] W. Teng, X. Ding, X. Zhang, Y. Liu, and Z. Ma, "Multi-fault detection and failure analysis of wind turbine gearbox using complex wavelet transform," *Renewable Energy*, vol. 93, pp. 591–598, 2016.

[8] S. Djurovic, C. J. Crabtree, P. J. Tavner, and A. C. Smith, "Condition monitoring of wind turbine induction generators with rotor electrical asymmetry," *IET Renewable Power Generation*, vol. 6, no. 4, pp. 207–216, 2012.

[9] Y. Wang, M. Liang, and J. Xiang, "Damage detection method for wind turbine blades based on dynamics analysis and mode shape difference curvature information," *Mechanical Systems and Signal Processing*, vol. 48, no. 1-2, pp. 351–367, 2014.

[10] X. An, D. Jiang, S. Li, and M. Zhao, "Application of the ensemble empirical mode decomposition and Hilbert transform to pedestal looseness study of direct-drive wind turbine," *Energy*, vol. 36, no. 9, pp. 5508–5520, 2011.

[11] S. J. Watson, B. J. Xiang, W. Yang, P. J. Tavner, and C. J. Crabtree, "Condition monitoring of the power output of wind turbine generators using wavelets," *IEEE Transactions on Energy Conversion*, vol. 25, no. 3, pp. 715–721, 2010.

[12] J. Igba, K. Alemzadeh, C. Durugbo, and E. T. Eiriksson, "Analysing RMS and peak values of vibration signals for condition monitoring of wind turbine gearboxes," *Renewable Energy*, vol. 91, pp. 90–106, 2016.

[13] X. D. Zhang, B. J. Xu, G. X. Wu, and Y. B. Zuo, "Research on fault diagnosis expert system of wind turbine," *Manufacturing Automation*, vol. 36, pp. 21–25, 2014.

[14] Z. L. Yang, B. Wang, X. H. Dong, and H. Liu, "Expert system of fault diagnosis for gear box in wind turbine," *Systems Engineering Procedia*, vol. 4, pp. 189–195, 2012.

[15] Y. K. Liu, S. Su, Y. Yang, and J. P. Yao, "Fault diagonsis approach for wind turbine based on signed directed graph," *Journal of Mechanical Strength*, vol. 35, no. 5, pp. 583–588, 2013.

[16] Y. Qian and R. Yan, "Gearbox fault diagnosis in a wind turbine using single sensor based blind source separation," *Journal of Sensors*, vol. 2016, Article ID 6971952, 14 pages, 2016.

[17] X. Liu, X. Xu, Z. Jiang, G. Wu, and Y. Zuo, "Application of the state deterioration evolution based on bi-spectrum entropy and HMM in wind turbine," *Chaos, Solitons & Fractals*, vol. 89, pp. 160–168, 2016.

[18] J. Wang, R. X. Gao, and R. Yan, "Integration of EEMD and ICA for wind turbine gearbox diagnosis," *Wind Energy*, vol. 17, no. 5, pp. 757–773, 2014.

[19] Y. Hu, X. T. Tu, F. C. Li, and G. Meng, "Joint high-order synchrosqueezing transform and multi-taper empirical wavelet transform for fault diagnosis of wind turbine

planetary gearbox under nonstationary conditions," *Sensors*, vol. 18, no. 2, pp. 150–167, 2018.

[20] R. Yan, Y. V. Qian, S. J. Hu, and R. X. Gao, "Wind turbine gearbox fault diagnosis based on wavelet domain stationary subspace analysis," *Journal of Mechanical Engineering*, vol. 50, no. 11, pp. 9–16, 2014.

[21] A. Adouni, D. Chariag, D. Diallo, M. Ben Hamed, and L. Sbita, "FDI based on artificial neural network for low-voltage-ride-through in DFIG-based wind turbine," *ISA Transactions*, vol. 64, pp. 353–364, 2016.

[22] X. Y. Wang, "Fault diagnosis on transmission system of wind turbines based on wavelet packet transform and RBF neural networks," *Applied Mechanics and Materials*, vol. 373–375, pp. 1102–1105, 2013.

[23] Z. Wang and S. Liu, "Study on synthesis fault diagnosis strategy of the brake system of wind turbine based on evidence theory," *Communications in Computer and Information Science*, vol. 226, pp. 18–25, 2011.

[24] A. Bechkaoui, A. Ameur, S. Bouras, and A. Hadjadj, "Open-circuit and inter-turn short-circuit detection in PMSG for wind turbine applications using fuzzy logic," *Energy Procedia*, vol. 74, pp. 1323–1336, 2015.

[25] H. Merabet, T. Bahi, and N. Halem, "Condition monitoring and fault detection in wind turbine based on DFIG by the fuzzy logic," *Energy Procedia*, vol. 74, pp. 518–528, 2015.

[26] Z.-X. Yang, X.-B. Wang, and J.-H. Zhong, "Representational learning for fault diagnosis of wind turbine equipment: a multi-layered extreme learning machines approach," *Energies*, vol. 9, no. 6, pp. 379–395, 2016.

[27] G.-B. Huang, X. Ding, and H. Zhou, "Optimization method based extreme learning machine for classification," *Neurocomputing*, vol. 74, no. 1–3, pp. 155–163, 2010.

[28] G.-B. Huang, D. H. Wang, and Y. Lan, "Extreme learning machines: a survey," *International Journal of Machine Learning and Cybernetics*, vol. 2, no. 2, pp. 107–122, 2011.

[29] W.-Y. Deng, Q.-H. Zheng, and Z.-M. Wang, "Cross-person activity recognition using reduced kernel extreme learning machine," *Neural Networks*, vol. 53, pp. 1–7, 2014.

[30] Y. J. Guo, *Research on Angular-Domain Vibration Signal Processing and Fault Diagnosis Methods for Wind Turbine Gearbox*, Zhejiang University, Hangzhou, Zhejiang, China, 2015.

[31] N. Sawalhi, R. B. Randall, and D. Forrester, "Separation and enhancement of gear and bearing signals for the diagnosis of wind turbine transmission systems," *Wind Energy*, vol. 17, no. 5, pp. 729–743, 2014.

[32] Z. Feng, S. Qin, and M. Liang, "Time-frequency analysis based on vold-kalman filter and higher order energy separation for fault diagnosis of wind turbine planetary gearbox under nonstationary conditions," *Renewable Energy*, vol. 85, pp. 45–56, 2016.

[33] S. Sheng, "Investigation of various wind turbine drivetrain condition monitoring techniques," in *Proceedings of the Wind Turbine Reliability Workshop*, Albuquerque, NM, USA, August 2011.

[34] F. Oyague, D. Gorman, and S. Sheng, "NREL gearbox reliability collaborative experimental data overview and analysis," in *Proceedings of the Windpower Conference and Exhibition*, Dallas, TX, USA, May 2010.

[35] S. Sheng, *Wind Turbine Gearbox Condition Monitoring Round Robin Study: Vibration Analysis*, National Renewable Energy Laboratory, Denver, CO, USA, 2012.

[36] D. L. Hall and J. Llinas, "An introduction to multisensor data fusion," *Proceedings of the IEEE*, vol. 85, no. 1, pp. 6–23, 1997.

[37] C. Pohl and J. L. Van Genderen, "Review article multisensor image fusion in remote sensing: concepts, methods and applications," *International Journal of Remote Sensing*, vol. 19, no. 5, pp. 823–854, 1998.

[38] G.-B. Huang, Q.-Y. Zhu, and C.-K. Siew, "Extreme learning machine: theory and applications," *Neurocomputing*, vol. 70, no. 1–3, pp. 489–501, 2006.

[39] Y. Q. Zhou, J. Xie, L. L. Li, and M. Z. Ma, "Cloud model bat algorithm," *Scientific World Journal*, vol. 2014, Article ID 237102, 11 pages, 2014.

[40] CSDN, 2013, https://download.csdn.net/download/xuemanxinhe/5098401?web=web.

[41] L. W. Zhang and J. S. Yuan, "Fault diagnosis of power transformers using kernel based extreme learning machine with particle swarm optimization," *Applied Mathematics & Information Sciences*, vol. 9, pp. 1003–1010, 2015.